Journal of Physics: Conference Series **123** (2008) 012012 doi:10.1088/1742-6596/123/1/012012

Comparison of the filament behaviour observed during type I ELMs in ASDEX Upgrade and MAST

A Kirk[1], A Herrmann[2], B Ayed[1,3], T Eich[2], H W Muller[2], G F Counsell[1], S Lisgo[1], M Price[1], A Schmid[2] , S Tallents[1,3] and H Wilson[4]

1 EURATOM/UKAEA Fusion Association, Culham Science Centre, Abingdon, Oxon OX14 3DB, UK
2 Max-Planck Institut für Plasmaphysik, EURATOM Association, Garching, Germany
3 Imperial College of Science, Technology and Medicine, University of London, London SW7 2BZ, UK
4 University of York, Heslington, York YO10 5DD UK

E-mail: Andrew.kirk@ukaea.org.uk

Abstract. A study of the evolution of the filaments observed during Type I ELMs on ASDEX Upgrade and MAST is presented. The filaments start off rotating toroidally/poloidally with velocities close to that of the pedestal. This velocity then decreases as the filaments propagate radially. On both devices the ion saturation current e-folding lengths of the filaments show a weak, if any, dependence on the size of the ELM ($\Delta W_{ELM}/W_{ped}$). On MAST the measured radial velocities of the filaments also show at most a weak dependence on $\Delta W_{ELM}/W_{ped}$.

1. Introduction

The energy released from the core plasma during Type I Edge Localised Modes (ELMs) is a key area of study for ITER [1], where the resultant power loadings, both inside and outside the divertor region, have an important impact on the choice of plasma facing materials. Although it is clear that filament structures exist during ELMs (see [2] and reference therein) it is still uncertain what parameters determine how much energy these filaments transport to the wall and what determines their size and how they propagate. This is mainly due to the lack of experimental data. If we can improve our understanding of at least some aspects of the ELM event, we may be able to reduce the uncertainty in the predictions for ITER.

In order to increase the data available that can be used to determine the parameters affecting the radial expansion of the filaments, IEA-ITPA co-ordinated experiments have been performed on MAST and ASDEX Upgrade. Initial studies investigated if the difference in the ion saturation current (I_{SAT}) e-folding length (λ_{ISAT}) observed on the two devices (ASDEX Upgrade: λ_{ISAT} ~ 2-2.5 cm MAST: λ_{ISAT} ~ 3-4 cm) could be due to the difference in the toroidal field and/or connection length in the machines. Scans were performed on both devices of B_T and I_P independently, keeping the plasma

density fixed, but no measurable change in λ_{ISAT} was observed [2]. In this paper, the results of scans over other plasma parameters are presented.

The layout of this paper is as follows: in section 2 new results on filament propagation will be presented. In section 3 a study of the radial efflux and the plasma parameters that may influence it will be discussed. In section 4 a simple simulation is used to illustrate how the radial motion of the filaments combined with parallel transport gives rise to the observed radial profiles.

2. Filament propagation

The poloidal/toroidal motion of the filaments determines the region of interaction of the filaments with the first wall/limiter, while their radial motion, energy content and loss mechanism determines the magnitude of the interaction. There is a general consensus that the dominant loss mechanism, once the filaments have separated from the LCFS, is through ion parallel processes. This is based on evidence from a number of sources, including: 1) that the divertor ELM energy flux rise time is correlated with the ion transport time [3], 2) that the particle content of the filaments decreases exponentially with distance from the LCFS and 3) that the electron temperature in the filament decreases more rapidly [4] than the ion temperature [5][6].

Direct observation of the toroidal motion of the filaments has been reported on MAST using fast visible imaging [7] [8]. These show that the filaments start off at the plasma edge rotating at the velocity of the pedestal. After 50-100 μs, the filaments decelerate toroidally and accelerate radially outwards. As the filaments propagate radially they follow the direction of the local field line and remain approximately constant in poloidal width.

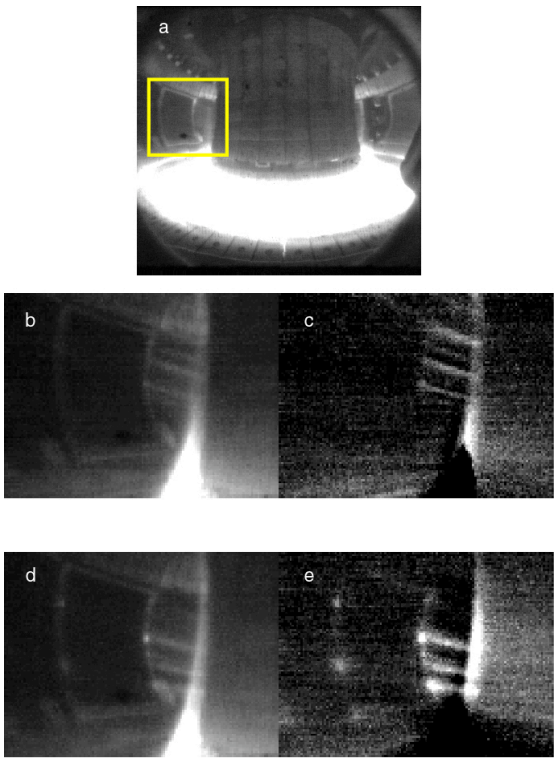

Figure 1 Visible images obtained on ASDEX Upgrade. a) full view of the plasma with the region of fast acquisition shown as a box. b) image obtained during the start of the rise time of the target D_α due to an ELM and d) an image obtained 50 μs later during the same ELM. c) and e) are background subtracted versions of b and d respectively.

Similar observations have recently been repeated on ASDEX Upgrade using the MAST Photron Ultima APX-RS camera. A wide angle view of the plasma was used as shown in figure 1a. In the analysis presented here, the reduced region (128×96 pixels) shown as the outlined box in figure 1a was recorded. This allowed images to be captured throughout the entire shot (5 s) at a frame rate of 90 kHz with an exposure time of 10 μs. In order to be able to track the filaments before they

interacted with in-vessel components a large gap (> 12cm) was used between the outboard plasma edge and the nearest limiter. In addition, to make the filaments more visible, deuterium gas puffing was used from the limiter in the region of view. Figure 1b shows an image obtained just after the start of the rise of the target D_α light associated with an ELM. Clear stripes are observed, which are on the outboard (low field side) edge of the plasma. In order to make the filaments more visible and to aid in analysis, a background subtraction is performed, which produces the image shown in figure 1c. Figure 1d and e show the original and background subtracted images obtained 50 μs (5 frames) later where the filaments have rotated toroidally in the co-current direction (or poloidally downwards) and 3 of the filaments have interacted with the ICRH limiter. The interactions show up as bright spots in the image.

In order to make the analysis of the motion quantitative, magnetic field lines in the Scrape Off Layer (SOL) have been projected on to the image. The filaments are observed to be aligned with the local field line; however, the pitch angle on ASDEX Upgrade at the mid-plane does not vary much with distance from the LCFS. Hence it is not possible to determine accurately the radial location of the filaments using such a technique. Only the mean radial velocity can be estimated by using the time that a filament takes from appearing until it reaches the limiter. The toroidal location and widths of the filaments are determined by calculating the intensity along each projected field line as a function of toroidal angle. The peaks observed in the derived distribution are then analysed to determine the widths and location of the filaments.

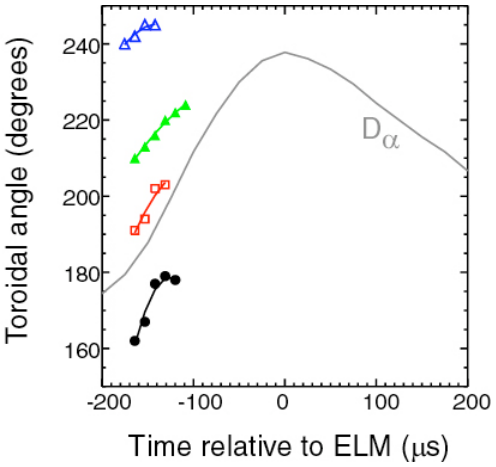

Figure 2 The toroidal angle of four filaments, tracked until they interact with the limiter, as a function of time during the ELM observed on ASDEX Upgrade. Superimposed is the divertor D_α signal.

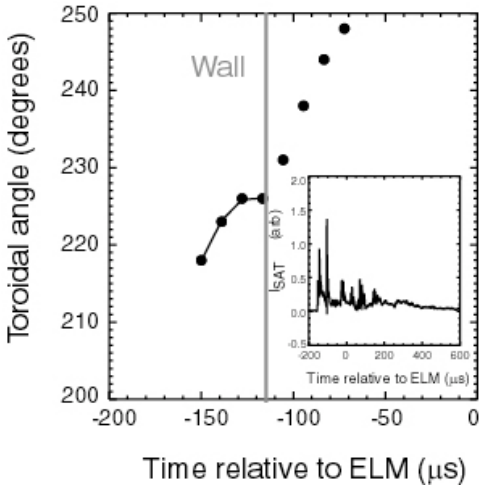

Figure 3 An example on ASDEX Upgrade of the toroidal angle of a filament as a function of time during the ELM for a filament that does not stop when it interacts with the limiter. The inset shows the ion saturation current measured by a Langmuir probe just in front of the limiter.

The width of the filaments perpendicular to the field line varies between 5 and 8 cm and as was observed on MAST [7], there is no evidence that the filament broadens as it travels out towards the limiter. The propagation of four filaments observed during a single ELM are shown in figure 2. The filaments reach the limiter ~ 120 μs before the peak in the divertor D_α light. This is consistent with the ion parallel transport timescales for this shot which is in the range 100 – 150 μs. The location of the filaments has been tracked in subsequent frames until they hit the limiter. All the filaments start off rotating toroidally in the co-current direction and after some time the toroidal rotation of an individual filament slows and soon afterwards hits the limiter. The toroidal location has been fitted as

a function of time to yield the initial toroidal velocity (which is in the range 10-30 kms^{-1}) and the toroidal deceleration (which is in the range (1-5)×10^8 ms^{-2}). Filaments are observed for up to 60 μs before hitting the limiter (12 cm distant), which gives a lower limit of the mean radial velocity of 2 kms^{-1}. However, on MAST the filaments are found only to leave the LCFS when the toroidal rotation slows [7][8]. If it was assumed that the same happened on ASDEX Upgrade then the transit time would decrease to < 30 μs and hence increase the mean radial velocity to > 4 kms^{-1}. Although the filaments are observed to hit the limiter, once they have made contact with it there is no evidence that they continue to propagate radially into the limiter shadow. This is consistent with the very fast fall off in the heat deposition on the side of the limiter observed in ASDEX Upgrade [9]. Hence the radial velocity of the filaments must reduce quickly on contact with the limiter.

If the filaments continue to be tracked after they contact the wall sometimes they stop but in other cases the filament motion changes once it has touched the wall and in fact its toroidal/poloidal motion increases again. This is illustrated in figure 3 in which a filament is tracked for 40 μs before interacting with the wall during which time its toroidal/poloidal motion decreases. However, in subsequent frames, a filament is observed to resume its toroidal motion. Whether this is the same filament or a field line lit up with material emitted from the limiter is not certain. This effect is observed to occur for ~ 20 % of the filaments. It occurs most frequently when the interaction with the limiter is strong or when the gap between the plasma edge and the wall is small. This suggests it is related to the energy content of the filament at the time it interacts with the limiter. It is not possible to identify the radial location of the filament, however, the interaction spot on the limiter is not observed to broaden, suggesting either that the energy content of the filament has been much reduced or that there is a radial gap between the filament and the limiter. These long lived "pseudo" filaments (i.e. they only exist because the original filament interacted with the limiter) could explain why the peaks in the I_{SAT} signal recorded by Langmuir probes near the limiter continue for up to 400 μs on AUG (see the inset in figure 3) and for up to 1 ms on JET [5] and also why the $E \times B$ determined velocities appear to decrease at large distance from the LCFS or in some cases become negative [10].

3. Parameters affecting the radial evolution

Rather than reporting individual filament motion the radial expansion of the filaments is often captured in terms of a radial e-folding length of particles and energy. In the simplest picture where the filaments propagate out radially with a constant velocity (V_r) and lose particles on ion parallel transport timescales ($\tau_{//} = L_{//}/c_s$, $L_{//}$ is the connection length and c_s the ion sound speed) then the particle e-folding length (λ) can be expressed as $\lambda \sim V_r\tau_{//} \sim V_rL_{//}/c_s$. The implications of an accelerating/decelerating filament will be discussed in the next section. To date the only direct measurement of the effect of plasma parameters on the e-folding length comes from DIII-D [4], which

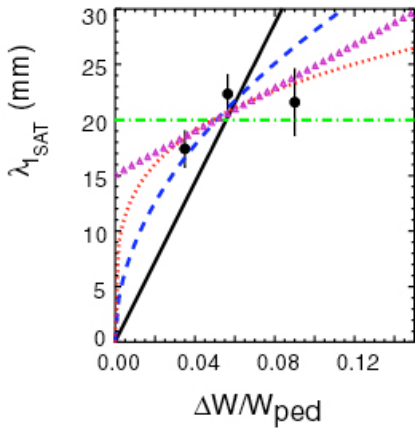

Figure 4 λ_{ISAT} as a function of $\Delta W/W_{ped}$ for data from ASDEX Upgrade. Superimposed on the figures are curves representing equation (1) with $\alpha = 0$ (dashed-dot), 0.25 (dashed), 0.5 (dotted) and 1 (solid). The triangles represent a fit to the form $\lambda = \lambda_{fil} + A \cdot (\Delta W / W_{ped})$.

has shown that the electron density e-folding length was found to depend on the density of the plasma having λ~3cm at high density and λ~10 cm at low density. In order to determine the power loading to the limiters, the power e-folding length is required. Previously, measurements on ASDEX Upgrade have shown that the e-folding length of the ion saturation current (λ_{ISAT}) measured by Langmuir probes is similar to that of the heat flux (λ_q) measured by infrared thermography [6]. In this paper measurements of the ion saturation current as a function of distance have been used to determine λ_{ISAT}, which is assumed to represent the power e-folding length of the radial efflux. The similarity between λ_q and λ_{ISAT} implies a large ratio of ion temperature to the electron temperature in the far SOL and indicates that the reduction of the energy content in the filament is due to convective losses [6].

In this paper we report results from recent studies in which scans have been performed over plasma parameters including ELM size and pedestal temperature produced by changing the density and/or the injected beam power. Figure 4 shows a plot of λ_{ISAT} on ASDEX Upgrade as a function of the fraction of the pedestal energy released by an ELM ($\Delta W_{ELM}/W_{ped}$). Although any dependence of the e-folding length is small compared to the scatter in the underlying data, a small increase in the e-folding length with $\Delta W_{ELM}/W_{ped}$ cannot be excluded. Previous analyses [11][12][13] have suggested that the dependence of the e-folding length should have the form:

$$\lambda \propto \left(\frac{\Delta W_{ELM}}{W_{ped}} \right)^{\alpha} \qquad (1)$$

Superimposed on figure 4 are curves representing equation (1) with $\alpha = 0$, 0.25, 0.5 and 1. From this data set alone it is difficult to rule out any of these dependencies, however, $\alpha = 1$ is highly unlikely.

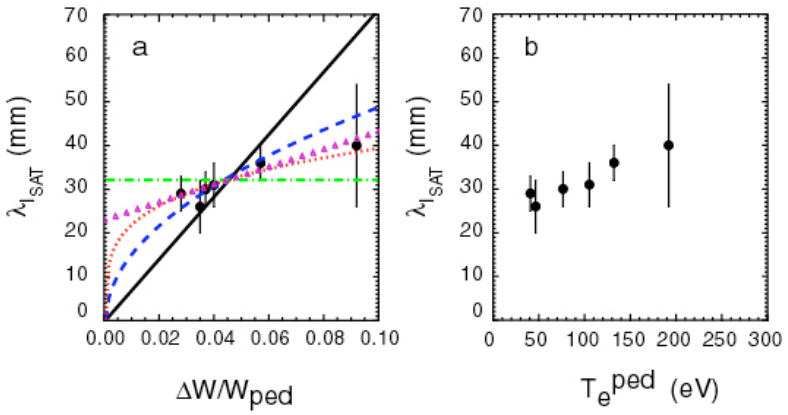

Figure 5 λ_{ISAT} as a function of a) $\Delta W/W_{ped}$ and b) T_e^{ped} for data from MAST. Superimposed on a) are curves representing equation (1) with $\alpha = 0$ (dashed-dot), 0.25 (dashed), 0.5 (dotted) and 1 (solid). The triangles represent a fit to the form $\lambda = \lambda_{fil} + A \cdot (\Delta W / W_{ped})$.

Similar measurements of λ_{ISAT} have been made as a function of plasma parameters on MAST. As can be seen from figure 5a and b there is a slight trend of increasing I_{SAT} e-folding length with increasing $\Delta W_{ELM}/W_{ped}$ and T_e^{ped} respectively. Superimposed on figure 5a are curves representing equation (1). The curve that gives the poorest description of the data is $\alpha = 1$. If it is assumed that a single value of α should be valid for the dependence of λ_{ISAT} on $\Delta W_{ELM}/W_{ped}$ in ASDEX Upgrade (figure 4) and MAST (figure 5a) then the best value of α is 0.25, although no dependence (i.e. $\alpha = 0$) cannot be ruled out. It is interesting to consider whether or not equation (1) has the correct form or whether, as may be indicated by the data, the correct form should have a constant term in addition to any dependence on ELM size i.e. $\lambda = \lambda_{fil} + f(\Delta W / W_{ped})$. Where λ_{fil} represents the initial radial dimension and distribution of energy within the filament. In this picture λ_{fil} would scale with the radial size of the filament. The triangles shown in figure 4 and 5a represent the results of a fit to the form $\lambda = \lambda_{fil} + A \cdot (\Delta W / W_{ped})$, which yields λ_{fil} = 15±3 mm (AUG) and 23 ±3 mm (MAST). In

reality the size of the filaments should not be treated as a constant off-set but should be convoluted with the radial motion of the filaments. Nevertheless it is interesting to note that the trend in λ_{fil} is similar to the trend in radial size of the filaments being smaller on ASDEX Upgrade (1-2cm) than on MAST (4-6 cm).

Note the higher $\Delta W_{ELM}/W_{ped}$ discharges in figure 5a have a higher T_e^{ped}. At higher temperatures the filament density should decrease more quickly due to parallel transport. This should then reduce the e-folding length, which is not observed in figure 5b. One explanation might be that the velocity (acceleration) of the filaments increases with T_e^{ped}. In order to investigate this further the velocity of the filaments has been measured directly by tracking the evolution of the filaments observed in the visible images for shots with different $\Delta W_{ELM}/W_{ped}$ and T_e^{ped}. As was reported in [8], although not all the filaments within a given ELM have the same size, the mean and sigma of the distribution of sizes does not change with $\Delta W_{ELM}/W_{ped}$ i.e. on average there is no evidence that larger ELMs have larger filaments. The radial location of each filament during an ELM has been found as a function of time. Since individual filaments leave the LCFS at different times [7][8], t_0 has been defined as the time at which each particular filament is last in contact with the LCFS. For each value of $\Delta W_{ELM}/W_{ped}$ the filaments in several ELMs have been tracked and the radial location (Δr_{LCFS}) of each filament as a function of time has been determined. The data have been binned in 10 μs time intervals relative to the t_0 for each filament. For each time period and each value of $\Delta W_{ELM}/W_{ped}$ the mean value and the R.M.S. of the distribution has been determined. Figure 6 shows a plot of the mean value of Δr_{LCFS} as a function of time relative to t_0 for filaments with low ($\Delta W_{ELM}/W_{ped} = 0.028$) and high ($\Delta W_{ELM}/W_{ped} = 0.092$) ELM energy losses. As can be seen, on average the filaments in ELMs with high $\Delta W_{ELM}/W_{ped}$ expand away from the LCFS faster than the ones at low $\Delta W_{ELM}/W_{ped}$. The radial expansion has been fitted according to a radial acceleration (solid curve) or constant velocity (dashed curve).

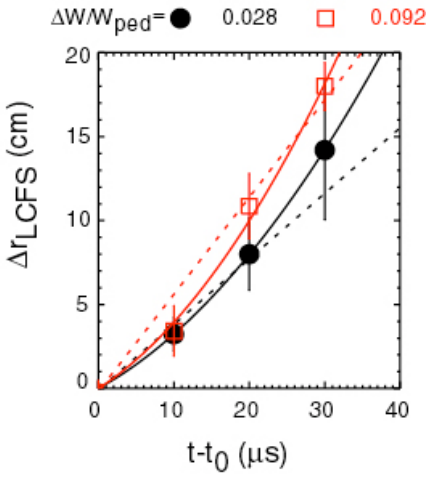

Figure 6 The radial distance of filaments from the LCFS (Δr_{LCFS}) as a function of time relative to the point at which the filament left the LCFS (t_0) for ELMs with $\Delta W/W_{ped}$ = 0.028 and 0.092 on MAST. The curves represent fits to the radial expansion as due to an acceleration (solid) or constant velocity (dashed).

Figure 7a shows a plot of the acceleration as a function of $\Delta W_{ELM}/W_{ped}$. Superimposed are curves representing $a_r \propto (\Delta W_{ELM}/W_{ped})^{\alpha}$ with $\alpha = 0$ (dashed-dot), 0.25 (dashed), 0.5 (dotted) and 1 (solid). The data are best described when $\alpha = 0.25$. Although the accelerating hypothesis best describes the underlying radial profiles, figure 7b plots the results of the fits assuming a constant velocity as a fraction of the ion sound speed versus $\Delta W_{ELM}/W_{ped}$. The general conclusion is that there is little evidence that the radial velocity as a function of the ion sound speed depends strongly on $\Delta W_{ELM}/W_{ped}$.

In reference [14] it is argued that the polarisation currents, present in the filaments, cannot be short-circuited through the targets because the parallel currents required exceed the ion saturation

current at the plates. This then leads to a prediction that the filaments will accelerate away from the edge of the plasma. The acceleration is determined by the balance between the ∇B drift current inside the filament and the polarization current in the SOL plasma. The impact of the polarization current is amplified by the distortion of the magnetic flux tube, especially near the X-point. The calculations show: 1) good agreement with the measured acceleration on MAST, 2) that as is observed [2], the accelerations should be larger on MAST than on ASDEX Upgrade and 3) predict that for a given magnetic configuration the acceleration $a_r \propto \frac{(T_i + T_e)}{R}$. Figure 7c shows a plot of the radial acceleration as a function of the pedestal electron temperature on MAST. There is a slight increase in a_r with T_e^{ped} but it is not linear (solid curve) as would be predicted in reference [14]. However, the data are compatible with a curve of the form $a_r = a_0 + f(T_e)$, with $a_0 \approx 1.3x10^8$ ms^{-2}. This initial drive term (a_0) may be due to the acceleration that is predicted in the non-linear ballooning mode theory [15].

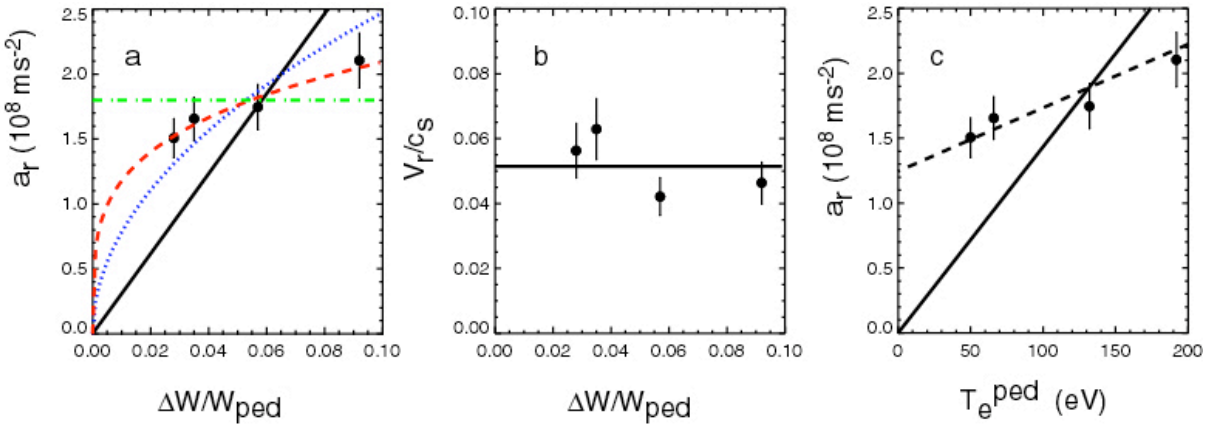

Figure 7 Analysis of the filaments observed in visible images on MAST. a) Radial acceleration as a function of $\Delta W/W_{ped}$, b) the radial velocity as a fraction of the sound speed as a function of $\Delta W/W_{ped}$ and c) radial acceleration as a function of the electron temperature pedestal.

4. Modelling the radial e-folding lengths and power loads

In order to get a better understanding of how the radial motion of, and parallel transport within, a filament gives rise to the observed radial decays a Monte Carlo simulation has been performed. Initially it is assumed that a filament has been created with length $2L$, uniformly populated with particles. Each particle has a velocity as derived from a Maxwellian velocity distribution according to an initial temperature and it is assumed that ion convective transport is dominant. Each particle is tracked until it leaves the end of the filament. As a function of time the number of particles and the mean absolute velocity of the particles within ±0.1 L of the centre of the filament are calculated to represent the density and ion temperature at the mid-plane of the filament. Figure 8a shows the number of particles at the mid-plane from two simulations for an ASDEX Upgrade like plasma with L = 10m and T_i = 500 and 1000 eV. The first thing that can be observed is that the number of particles at the mid-plane remains approximately constant for 15 (25) ms for the high (low) temperature case. This is because during this period there are effectively the same numbers of particles entering the middle section as are leaving it and it is only after this time that the loss out of the top and bottom of

the filament plays a role at the mid-plane. This effect was also observed in the more refined kinetic modelling shown in figure 2 of reference [16].

If it is now assumed that the filament moves with a constant radial velocity of 1 kms^{-1} this would then lead to the radial profiles of ion saturation current (calculated by multiplying the density by the square root of the temperature i.e. ignoring the electron temperature which is assumed to be much less than the ion temperature) shown in figure 8b. The profiles show an exponential decay for values of Δr_{LCFS} > 3cm, with λ_{ISAT} similar to that observed in the data (this was made possible by choosing V_r = 1kms^{-1}). However, in addition to the exponential decay, at small Δr_{LCFS} a flat region is produced which is not observed in the data. This could indicate that either the initial assumptions of the model are incorrect (e.g. the filament is not uniformly filled along its length) or the filament is filled but does not separate from the LCFS for some time after formation or that there is some loss mechanism missing in the model or because the filaments do not travel with a constant radial velocity but accelerate away from the LCFS.

If instead of a constant velocity, the filaments are assumed to accelerate away from the LCFS with a = 3x10^7 ms^{-2} or to decelerate according to the measurements of the electric field on DIII-D [4] then the radial profiles for the ion saturation current shown in figure 8c and d respectively are produced. In the case of the acceleration (figure 8c) the filament now spends longer initially at small values of Δr_{LCFS} and so instead of producing a flat region it produces profiles that would be best fit with two exponentials, similar to what has been observed in data from JT-60U [17]. In contrast the decelerating filament still produces a flat initial region but then falls off much more quickly than the measured e-folding lengths.

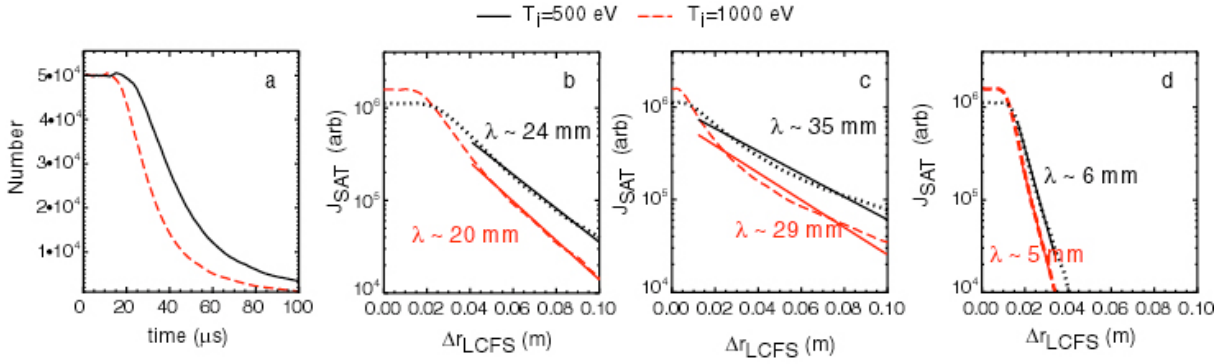

Figure 8 a) the evolution of the particles at the mid-plane as a function of time within a simulated filament with two temperatures. The radial distribution of the ion saturation current at the mid-plane for a simulated filament b) moving with a constant radial velocity of 1 kms^{-1}, c) accelerating radially with a = 3x10^7 ms^{-2} and d) decelerating from an initial velocity of 800 ms^{-1}.

The double exponential structure predicted for the accelerating filaments makes comparison with the single exponential fits applied to the data difficult. However, fits to the region of Δr_{LCFS} > 2 cm with a single exponential, give e-folding lengths that are similar but slightly larger than those observed experimentally. They could be improved by a better choice of the acceleration or the length of the filament; however, this amount of tuning would not be justified given the simplicity of the model.

In order to make a quantitative prediction for the amount of power arriving outside the divertor using a simulation of the kind described above, in addition to the information on the size and motion of the filament, a knowledge of how much energy is in the filament at the time it separates from the LCFS is needed. On MAST the radial density and electron temperature profiles of filaments, obtained from Thomson scattering, have been combined with the measured perpendicular size and the assumption that the filament extends between upper and lower X-points to calculate the energy content

assuming $T_i = T_e$ [18]. The maximum energy content of a single filament, observed close to the LCFS, is 2.5 % of ΔW_{ELM}.

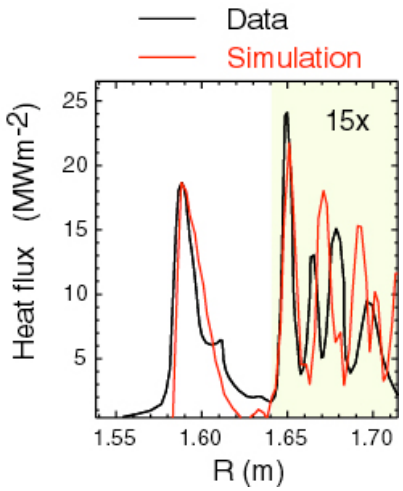

Figure 9 The simulated and observed divertor target radial power profile based on the observed evolution of the filaments.

There are large error bars on these numbers due to the uncertainties in the volume of the filament and the unknown ion temperature. However, they have been used as input to a Monte Carlo simulation of the power arriving at the divertor target in MAST [8]. On MAST, the first wall/limiter is a long way from the plasma and hence effectively all the energy released by an ELM arrives at the divertor. In order to test the validity of this model it would be better to simulate a device such as ASDEX Upgrade which has made measurements of the power due to the filaments arriving at the remote parts of the target [19] and limiters [9]. The simulation assumes T_i = 500 eV and starts off with 12 filaments each with an oval cross section with 2cm radial extent and 6cm in the perpendicular direction. For a period of 50 μs these filaments rotate with the pedestal velocity and release particles into the SOL. After this time individual filaments decelerate toroidally and accelerate away radially (with $a_r = 3\text{x}10^7$ ms^{-2}), each carrying up to 2.5 % of the total number of particles lost. As these filaments move radially, the particles are tracked until they reach the divertor target or interact with the wall which is located at a distance of 4 cm from the plasma edge. The number and velocity distribution of the particles arriving at the target and/or wall are used to calculate the effective power density profile that would be observed during the integration time of the infrared cameras. The resulting target profile at a particular toroidal location, chosen to best agree with the experimental data, is shown in figure 9. Note in the experimentally measured data the power density is artificially increased by a factor of 15 in the region $R > 1.64$ m due to a surface layer on the tile in this region [19] and therefore, for comparison, the simulation has also been increased by the same factor in this region. The size and number of the structures are similar to the observed profiles. The computed profile varies with toroidal location and the experimental one from ELM to ELM. In order to calculate the amount of energy arriving in the remote part of the target ($R > 1.64$m) the experimental data has been averaged over 20 ELMs and the model data has been averaged toroidally. The result is that 7 % is predicted from the simulation compared to the 5 % measured. In order to calculate the amount of energy arriving at the limiter a 2-D profile of the AUG limiter has been incorporated into the model. If a particle in the filament intercept with the limiter before arriving at the target its energy is assumed to have been deposited at the limiter. The energy deposited on the limiter is 18 % in the simulation compared to the 25 % measured using IR [9].

5. Summary

In this paper results from ASDEX Upgrade and MAST on the propagation of filaments observed during type I ELMs have been presented. The new images obtained on ASDEX Upgrade show how the filaments start off rotating toroidally in the co-current direction and after sometime the toroidal rotation of an individual filament slows and soon afterwards it hits the limiter (12 cm from the LCFS). Although it is not possible to track the radial position of the filaments directly they are observed for up to 60 μs before hitting the limiter, which gives a lower limit of the mean radial velocity of 2 kms^{-1}. Once the filament interacts with the nearest limiter then it is more difficult to predict its evolution. On both devices the ion saturation current e-folding lengths of the filaments show a weak, if any, dependence on the size of the ELM ($\Delta W_{ELM}/W_{ped}$). On MAST the measured radial velocities of the filaments show at most a weak dependence on $\Delta W_{ELM}/W_{ped}$. The results from a simple model based on parallel transport have been presented and shows the effect that the different radial propagation hypotheses have on the fall-off length. This model has also been used to explain the amount of power arriving at the remote parts of the target and first wall for a single shot in ASDEX Upgrade. However, it should be stressed that such models need to be refined and tested on other discharges at different $\Delta W_{ELM}/W_{ped}$ and on other devices.

Acknowledgement

UKAEA authors were funded jointly by the United Kingdom Engineering and Physical Sciences Research Council and by the European Communities under the contract of Association between EURATOM and UKAEA. The views and opinions expressed herein do not necessarily reflect those of the European Commission.

References

[1] Loarte A *et al*. 2002 *Plasma Phys. Control. Fusion* **44** 1815
[2] Kirk A *et al*. 2005 *Plasma Phys. Control. Fusion* **47** 995
[3] Eich T *et al*. 2005 *J. Nucl. Mater.* **337-339** 669
[4] Boedo J A *et al*. 2005 *Phys. Plasmas* **12** 072516
[5] Pitts R A *et al*. 2006 *Nucl. Fusion* **46** 82
[6] Herrmann A *et al*. 2007 *J. Nucl. Mater.* **363-365** 528
[7] Kirk A *et al*. 2006 *Phys. Rev. Lett.* **96** 185001
[8] Kirk A *et al*. 2007 *Plasma Phys. Control. Fusion* **49** 1259
[9] Herrmann A *et al*. 2004 *Plasma Phys. Control. Fusion* **46** 971
[10] Silva C *et al*. 2005 *J. Nucl. Mater.* **337-339** 722
[11] Loarte A *et al*. 2006 *Proc. Of 21st IAEA Fusion Energy Conf. (Chengdu)* IAEA-CN-149/IT/P1-14
[12] Fundamenski W and Pitts R A 2007 *J. Nucl. Mater.* **363-365** 319
[13] Eich T *et al*. 2007 *Plasma Phys. Control. Fusion* **49** 573
[14] Rozhansky V and Kirk A 2008 *Plasma Phys. Control. Fusion* **50** 025008
[15] Wilson H R and Cowley S C 2004 *Phys. Rev. Lett.* **92** 175006
[16] Fundamenski W *et al*. 2004 *Phys. Control. Fusion* **46** 259
[17] Asakura N *et al*. 2005 *J. Nucl. Mater.* **337-339** 712
[18] Scannel R *et al*. 2007 *Plasma Phys. Control. Fusion* **49** 1431
[19] Eich T *et al*. 2003 *Phys. Rev. Lett.* **91** 195003